# The Influence of Y-Axis Variables on Tunnel Piston Effect Measurements in 3D Models Simplified to 2D

Dito Afandi[1]*, Taqia Rahman[1], Latif Budi Suparma[1]
[1]Department of Civil and Enviromental Engineering, Universitas Gadjah Mada, Yogyakarta, INDONESIA
**Corresponding author:* ditoafandi@mail.ugm.ac.id

## ABSTRACT

The 3D CFD simulation requires a lot of resources, making expensive predictions. This research uses a 2D model to simplify 3D model simulation that previous researchers have studied while keeping x-axis airspeed variation forecasting accuracy. This study aims to analysis the 2D positioning effect of monitoring points in y-axis variables as representation of velocity transducer in 3D model. The 3D model was scaled 1/20 and simplified by using hydraulic diameter and blockage ratio to calculate train and tunnel widths. The modelling is using the SIMPLE, k-$\varepsilon$ standard model, 0.04 m mesh size, and CFL number 0.75. Four variables are placed in the middle position of the tunnel, a distance of 50 mm from the middle of the tunnel up and down, and on the tunnel wall. The results show that placing the measurement point in the middle of the tunnel better represents the x-axis airspeed measured at the centre point of the cross section of the inlet and outlet tunnel. This model is validated, which achieves MBE values of 3.9% and 4.5% for the inlet and outlet velocity ratios, respectively.

Keywords: Pressure wave, Model simplification, Dynamic mesh layering, Uncompressible flow, Compressible flow.

## 1 INTRODUCTION

The operation of a train with higher speed requires particular attention to be paid to the flow of air surrounding the train, particularly when the train is traveling through the tunnel. The airflow around the trains, which is commonly referred to as a slipstream, is generated by train can produce turbulent and dynamic air flows with substantial pressure and velocity magnitudes. These air flows possess the capability to interact with and potentially disrupt objects and individuals in close proximity to the tracks (Jordan et al. 2009). As an illustration, the slipstream exerted a force on the luggage barrow, causing it to be pushed. The object collided with the moving train and was then flung across the platform (Johnson et al. 2001).

The majority of research modelling train and tunnel interactions utilises 3D model. The modelling of this 3D model involves a large amount of elements. Furthermore, because the train moves at higher speed, the necessary time step is quite small. Consequently, investigating the train and tunnel connection requires significant resources, such as processing power from supercomputer, and large data handling.

Method used in previous research (M.Liu et al. 2018) involves converting the 3D representation of the tunnel and train, which are in the form of a box, into a top-down view that illustrates the link between the train and the tunnel. After considering many comparisons, it is determined that the width of the tunnel is determined by the hydraulic diameter, whereas the width of the train is determined by the blockage ratio.

This study seeks to compare the impact of the varied position of the measurement point on the y-axis on the x-axis airspeed in the tunnel piston effect.

## 2 METHODOLOGY

### 2.1 Remodelling Concept of Transforming 3D Model Into 2D Model

Prior researchers have investigated methods to simplify the modelling of moving object traversing tunnels. In their study, M. Liu et al. (2018) assessed the correctness of the 3D model by comparing it with the results of the experiment. The researchers simplify the modelling process for a basic rectangular item transitioning from a fixed position to movement within a tunnel. The study suggested that the width dimension of the 2D tunnel model is determined based on the hydraulic diameter of the tunnel, whereas the width dimension of the 2D train model is determined based on the blockage ratio. The two width dimensions refer to the measurements of the tunnel and train when observed from the top-down view. In order to obtain a 2D model, a top view of the 3D model is created. The length dimensions of

the tunnel and the train correspond to the actual length of the objects. Figure 2-1 is an example of how 3D geometric measurements are converted into 2D geometric measurements.

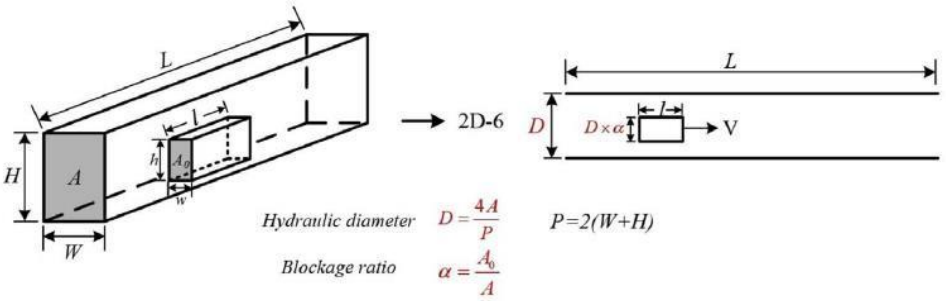


Figure 2-1. Conversion scheme of a 3D model to a 2D model (M. Liu et al. 2018).

The hydraulic diameter ($D$) is determined by applying equation (1).

$$D = {}^{4A}/_{P} \quad (1)$$

The cross-sectional area ($A$) of the tunnel is calculated by multiplying the actual height ($H$) and the actual width ($W$) of the tunnel face. The perimeter of the tunnel face cross-section, denoted as ($P$), can be determined by adding twice the real tunnel height ($H$) and twice the actual tunnel width ($W$). The hydraulic diameter value serves as the width of the tunnel in the 2D model geometry. The blockage ratio equation ($\alpha$) is determined by utilising equation (2).

$$\alpha = {}^{A_o}/_{A} \quad (2)$$

The cross-sectional area of the train ($A_o$) is calculated by multiplying the height ($h$) and width ($w$) of the front cross-section of the train. The width of 2D train ($d$) is determined by utilizing equation (3).

$$d = D.\alpha \quad (3)$$

This study validate a comparison between the ratio of x-axis airspeed ($U$) with maximum train speed ($U_{Tmax}$=3 m/s) obtained from velocity transducers positioned at the entry and exit of the tunnel. These measurements were then compared with result of a three-dimensional modelling approach by Kim and Kim (2007) which shown in Figure 2-2.

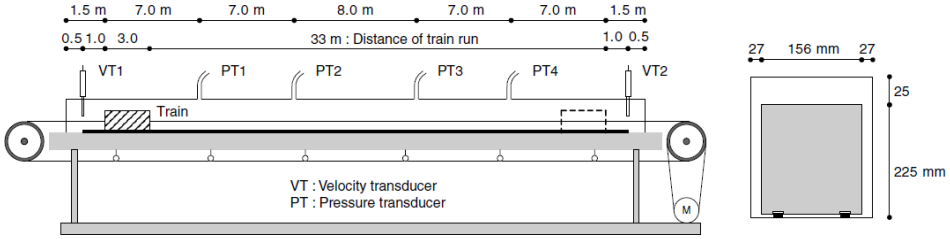


Figure 2-2. Experimental design for studying the movement of an object within a tunnel (Kim and Kim 2007).

The results of transforming a 3D object geometry into a 2D object are shown in Table 2-1.

Table 2-1. The transformation dimension of the geometry of a 3D model into a 2D model by M. Liu et al. (2018).

| | 3D Geometry (mm) | 2D Geometry (mm) |
|---|---|---|
| Width of tunnel ($W$) | 210 | 228 |
| Height of tunnel ($H$) | 250 | - |
| Length of tunnel ($L$) | 39000 | 39000 |
| Width of train ($w$) | 156 | 152 |
| Height of train ($h$) | 225 | - |
| Length of train ($l$) | 3000 | 3000 |

## 2.2 Defining mesh, boundary conditions, and numerical solutions

Three types of dynamic mesh approaches can be used to model the moving objects: smoothing, layering, and remeshing. This study uses the dynamic mesh layering method to simulate the behaviour of moving objects. Thus, the 2D model is divided into multiple sections within the tunnel, namely three zones: the zone surrounding the train, the zone before the train, and the zone after the train, as shown in Figure 2-3. The zone closest to the train's surface is the targeted area for obtaining highly precise outcomes, necessitating improved mesh quality. The zones before and after the train are considered additional zones, allowing for the selection of the desired mesh quality. Meanwhile, using the same speed conditions as the experiment, a User-Defined Function (UDF) moves the object.

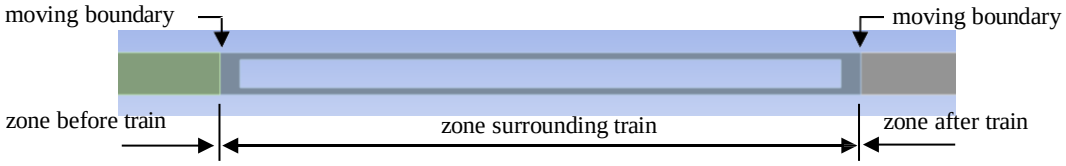


Figure 2-3. Moving boundary zone of the train

The configuration of the model uses mesh size of 0.04 m. The tunnel inlet and outlet are defined as a pressure inlet and outlet (*Pstatic=0*), allowing air to enter and exit the tunnel zone at a certain pressure. The wall interface is defined as no slip on the tunnel wall and on the train surface. Incompressible flow is commonly employed in basic fluid modelling when fluid velocities are modest, typically with Mach numbers below 0.3. The calculation of the necessary time step is accomplished by employing the Courant–Friedrichs–Lewy (CFL) condition number. In order to satisfy the CFL condition, the time step value in the numerical simulation must be less than or equal to the mesh size. In order to obtain a numerical solution that is both convergent and accurate, it is necessary for the CFL number to be less than or equal to 1. The maximum time step required with a mesh size of 0.04 and a velocity of 3 m/s is 0.0133. In this modelling, a time step of 0.01 is utilized as an initial value, which is calculated from CFL number of 0.75. Boundary condition of this model are shown in Figure 2-4

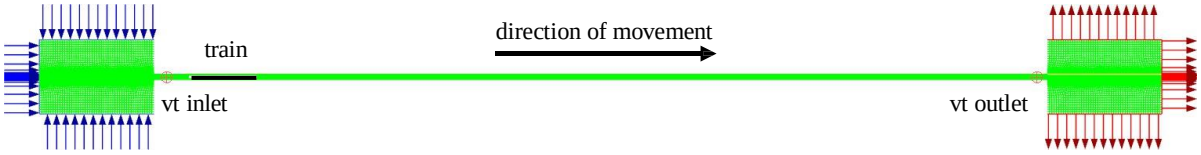


Figure 2-4. Boundary condition of the model and position of the velocity transducer (vt) in the tunnel inlet and outlet at x-axis.

The modelling has been calculated using the numerical parameters presented in the Table 2-2.

Table 2-2. Numerical parameters used for validation

| Parameter | Numerical Validation Parameters |
|---|---|
| CFD Software | Fluent (Ansys 2023 R2 Teaching) |
| Solver type | Pressure-based |
| Model | $k-\varepsilon, standard$ |
| | $C_\mu = 0.09$, $C_{s1} = 1.44$, $C_{s2} = 1.92$, $\sigma_k = 1$, $\sigma_s = 1.3$ |
| Fluid material | Constant air |
| Discretization schemes: | |
| Pressure | Second order |
| Momentum | Second order |
| Turbulent kinetic energy | Second order |
| Turbulent dissipation rate | Second order |
| Algorithm | SIMPLE |
| Time derivative | First order implicit |
| Initialization | Standard initialization method |

### 2.3 Monitoring point of velocity transducer

The y-axis distance between the model and the axis of symmetry of the tunnel is computed using a number of different variables in order to ensure that the results are correct. The following is a breakdown of the y-axis distance variables that are included in the two-dimensional model:

a. Y-axis, 0 or equal to the axis of symmetry of the 2-dimensional tunnel model
b. Y-axis, 50 mm
c. Y-axis, -50 mm
d. Y-axis, 114 mm or equal to the wall of the 2-dimensional tunnel model

## 3 RESULT AND DISCUSSION

### 3.1 Effect of Differences in Y-Axis Position on X-Axis Airspeed

Figure 3-1 and Figure 3-2 depict graphs of airspeed measurements along the x-axis recorded at the tunnel inlet when the train starts motion, corresponding to the graph of variations in train speed. The airspeed graph is quantified using various measurements on the y-axis, particularly at the centre axis (vt inlet or outlet x mid), at a distance of 050 mm on the positive axis or 43.86 percent of the centre axis (vt inlet or outlet x mid2), at a distance of 50 m on the negative axis or 43.86 percent of the centre axis (vt inlet or outlet x mid3), and along the tunnel wall (vt inlet or outlet x wall). The train speed indicated by the long dash line represents a graph of the intended train speed pattern, established by a user-defined function (UDF). This graph aligns with the velocity graph utilized in the research conducted by Kim and Kim (2007). The x-axis velocity at the inlet or outlet is represented by four continuous lines illustrating the airspeed at the four measurement spots.

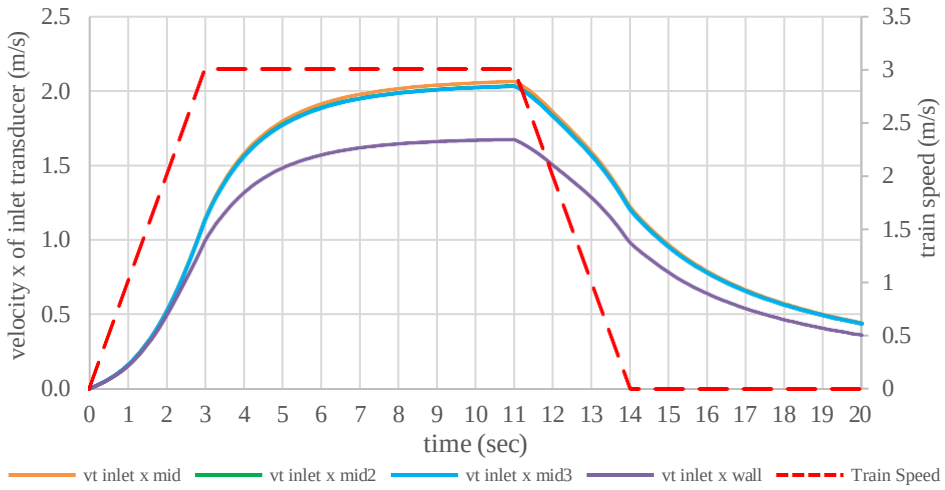


Figure 3-1. Graph of variation of x-axis velocity against time at the vt inlet; graph of variation of train speed against time in secondary y-axis.

Moreover, as the train initiates movement with an acceleration of 1 m/s², the airspeed at the inlet tunnel significantly escalates. Once the maximum train speed is reached, the x-axis velocity at the inlet gradually increases with a smoother curve until it reaches the maximum point before the train decelerates. The inlet x-axis velocity decreases in accordance with the train's decreasing speed. The airspeed continued to drop despite the train being motionless at the 14th second. The airspeed graph illustrates an obvious discrepancy when comparing the placement of the velocity transducer at the centre of the y-axis to its positioning on the tunnel wall. Despite the no-slip condition on the wall, the airspeed has dropped significantly. The no-slip wall condition effectively characterizes the behaviour of fluid motion within the domain. Specific friction coefficient values can be taken into account for precise measurement circumstances on tunnel walls. Simultaneously, the airspeed at vt inlet x mid2 and vt inlet x mid3 presents similar graphs, with a minor velocity discrepancy compared to vt inlet mid. This velocity disparity aligns with the principle of airflow proceeding in the same direction inside the domain.

Similar to the inlet velocity, when the train initiates movement with an acceleration of 1 $^{m}/_{s}^{2}$, the airspeed at the tunnel exit also experiences a significant increase, corresponding to the pattern of the inlet velocity until the 20th second. However, a discrepancy exists in the outlet velocity value recorded on the tunnel wall prior to the 14th second. Upon the train's stop of movement at the 14th second, the outlet velocity displayed a minor increase followed by a following reduction. The airspeed graph illustrates an obvious discrepancy when comparing the placement of the velocity transducer at the midpoint of the y-axis to its position on the tunnel wall. The airspeed measurements at vt x outlet mid, vt x outlet mid2, and vt x outlet mid3, which coincide, show a substantial variation from the inlet velocity.

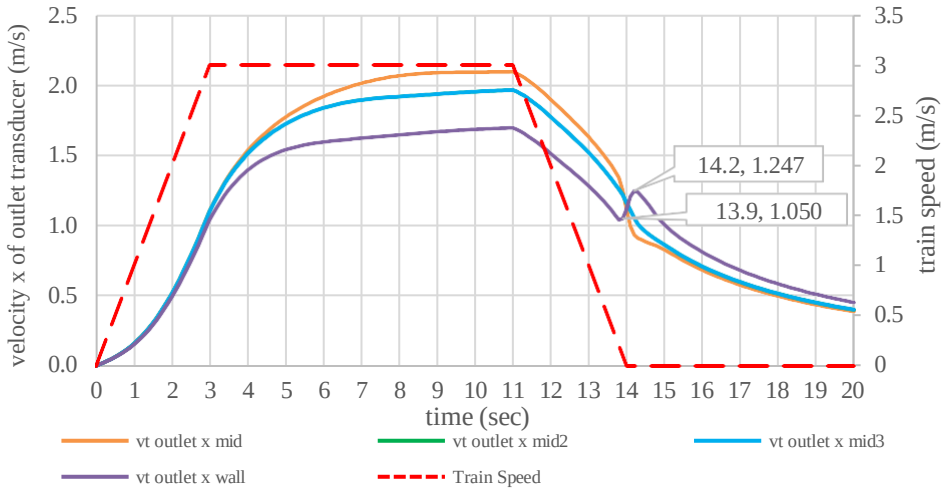


Figure 3-2. Graph of variation of x-axis velocity against time at the vt outlet; graph of variation of train speed against time in secondary y-axis.

Finally, the effect of the transducer's placement on airspeed when compared to the experimental and numerical values measured by Kim and Kim (2007) could be analysed in the next sub-chapter.

## 3.2 Parameter Validation of Proposed Model of Transforming 3D Model to 2D Model

The choice of dynamic mesh layering was based on its ease of setup, as mesh updates are limited to occur only between zones, while maintaining the same mesh form and point placements within zones. The mesh configuration in surrounding areas of the train will remain unchanged.

The x-axis airspeed measurement of the velocity transducer (vt) inlet and velocity transducer (vt) outlet was measured at regular intervals of 0.1 seconds at both the tunnel inlet and outlet. Then, the ratio of x-axis airspeed with maximum train speed illustrated in Figure 3-3 and Figure 3-4.

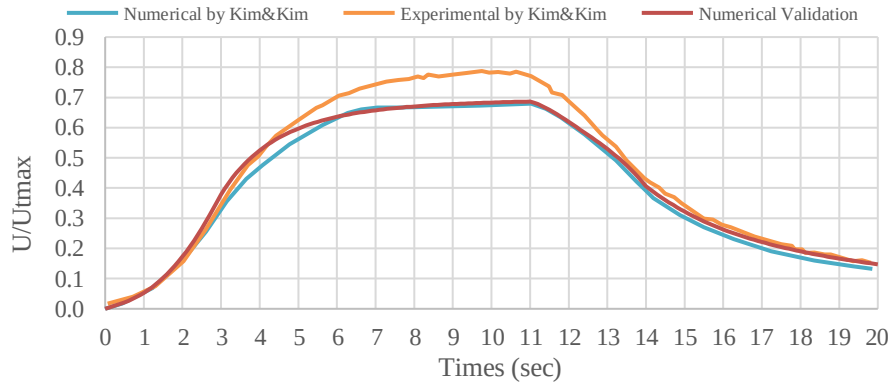


Figure 3-3. Comparison graph of velocity ratio of x-axis airspeed in inlet to maximum train speed ($U_{Tmax}$).

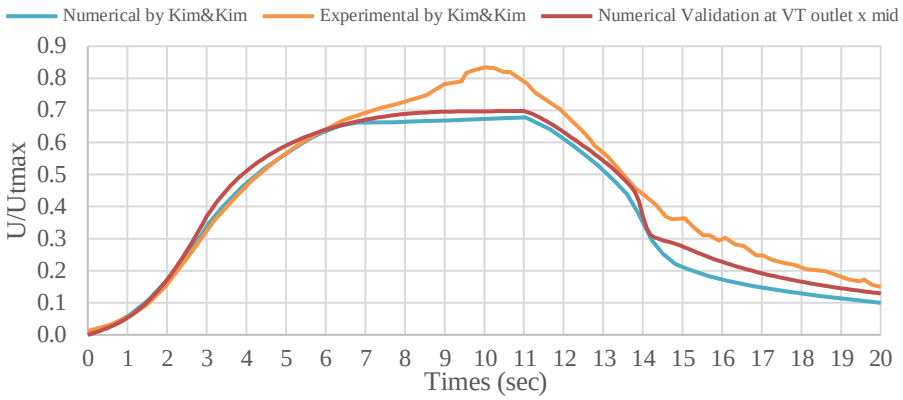


Figure 3-4. Comparison graph of velocity ratio of x-axis airspeed in outlet to maximum train speed ($U_{Tmax}$).

The MBE technique was utilized for validation of airspeed ratio by experimental results. The MBE correlation value was calculated via the online calculator provided by AgriMetSoft using 68 data points for the vt inlet x mid and 62 data points for the vt outlet x mid. The MBE results for vt inlet x mid and vt outlet x mid are -0.039 and -0.045, respectively. The MBE value of -0.039 and -0.045 indicates that the model is underestimated by 3.9% and 4.5%, meaning that the model prediction is 3.9% and 4.5% less than the actual observed value. The forecast model exhibits a subtle negative inclination. These two values can be accepted with more than 95% confidence level. So that the parameters utilized during the modelling provide an initial basis for following model.

## 4 CONCLUSION

The standard k-$\varepsilon$ model, employing the SIMPLE algorithm, is utilised to visualise unsteady turbulent flow conditions, incorporating a second-order equation for turbulent kinetic energy and turbulent dissipation rate, alongside a first-order implicit method for time derivatives and standard initialisation. In the context of modelling dynamic objects, dynamic mesh layering demonstrates simplicity in configuration and consistency in mesh quality. This approach also can be employed to enhance the efficiency of the resources required for modelling. The placement of the velocity transducer at the centre point of the 3D inlet tunnel cross section can be represented by placing the measurement point at the centre point of the tunnel or on the y-axis in this 2D model. These parameters are already validated with a 95.5-96.1 % confidence level. So that the parameters utilised during the modelling provide an initial basis for following model.

## ACKNOWLEDGEMENT

The authors acknowledge the computational and software resources provided by School of Civil Engineering, University of Leeds, UK.

## REFERENCE

Jordan, S.C., Sterling, M. and Baker, C.J. (2009). “Modelling the response of a standing person to the slipstream generated by a passenger train”. *Proceedings of the Institution of Mechanical Engineers, Part F: Journal of Rail and Rapid Transit*, 223(6), pp.567–579.

Johnson, T., Dalley, S. and Temple, J. (2001). *Recent Studies of Train Slipstreams*.

Kim, J.Y. and Kim, K.Y. (2007). “Experimental and numerical analyses of train-induced unsteady tunnel flow in subway”. *Tunnelling and Underground Space Technology*, 22(2), pp.166–172.

Liu, M., Zhu, C., Cui, T., Zhang, H., Zheng, W. and You, S. (2018). “An alternative algorithm of tunnel piston effect by replacing three-dimensional model with two-dimensional model”. *Building and Environment*, 128, pp.55–67.